Measurements of the Magnetic Flux Density in Steel Blocks of the CMS Magnet Yoke with the Solenoid Coil Fast Discharges

Vyacheslav Klyukhin *, Benoit Curé, Andrea Gaddi, Antoine Kehrli, Maciej Ostrega, Xavier Pons

Posted Date: 28 October 2024

doi: 10.20944/preprints202410.2201.v1

Keywords: electromagnetic modelling; magnetic flux density; superconducting coil; flux loops; magnetic field measurements; eddy current analysis; rotational symmetry; CMS detector magnet

Article

Measurements of the Magnetic Flux Density in Steel Blocks of the CMS Magnet Yoke with the Solenoid Coil Fast Discharges

Vyacheslav Klyukhin [1,2,3,*], Benoit Curé [2], Andrea Gaddi [2], Antoine Kehrli [2], Maciej Ostrega [2] and Xavier Pons [2]

[1] Skobeltsyn Institute of Nuclear Physics, Lomonosov Moscow State University, RU-119991, Moscow, Russia
[2] CERN, CH-1211, Geneva 23, Switzerland
[3] Joint Institute for Nuclear Research, RU-141980, Dubna, Moscow Region, Russia
* Correspondence: vyacheslav.klyukhin@cern.ch

Abstract: The general-purpose Compact Muon Solenoid (CMS) detector at the Large Hadron Collider (LHC) at CERN studies a production of new particles in the proton-proton collisions at the LHC center of mass energy 13.6 TeV. The detector includes the magnet based on the 6 m diameter superconducting solenoid coil operating with the current of 18.164 kA. This current creates a central magnetic flux density of 3.8 T that allows to measure momenta of the produced in collisions charged particles with tracking and muon subdetectors at a high precision. The CMS magnet contains a 10,000 ton flux-return yoke made of construction steel that bends muons in steel blocks magnetized with the solenoid returned magnetic flux. To reconstruct the muon trajectories, and thus, to measure the muon momenta, the drift tube and cathode strip chambers are located between the layers of the steel blocks and serve for this purpose. To describe the distribution of the magnetic flux in the magnet yoke layers, a three-dimensional computer model of the CMS magnet is used. To prove the calculations, the special measurements are performed with the flux loops wound in 22 cross-sections of the flux-return yoke blocks. The measured voltages induced in the flux loops during the CMS magnet ramp ups and downs, as well as during the superconducting coil fast discharges with the 190 s time constant, are integrated over time to obtain the initial magnetic flux densities in the flux loop cross-sections. The measurements obtained during the seven standard ramp downs of the magnet have been analyzed in 2018. From that time three fast discharges have occurred during the standard ramp downs of the magnet. This allows to single out the contributions of the eddy currents, induced in steel, to the flux loop voltages registered during the fast discharges of the coil. Accounting for these contributions to the flux loop measurements during manually triggered fast discharges in 2006 allows to perform the validation of the CMS magnet computer model with a better precision. The technique of the flux loop measurements, and the obtained results are presented and discussed.

Keywords: electromagnetic modelling; magnetic flux density; superconducting coil; flux loops; magnetic field measurements; eddy current analysis; rotational symmetry; CMS detector magnet

1. Introduction

The Compact Muon Solenoid (CMS) multi-purpose detector [1] at the Large Hardon Collider (LHC) [2] registers the charged and neutral particles created in the proton-proton collisions at a center of mass energy 13.6 TeV. The detector includes a 6 m diameter superconducting solenoid coil [3] with a length of 12.5 m and a central magnetic flux density B_0 of 3.81 T that is created by the operational direct current of 18.164 kA. Inside the superconducting coil around the interaction point of proton beams the major particle subdetectors are located: a silicon pixel and strip tracking detectors to register the charged particles; a solid crystal electromagnetic calorimeter to register electrons, positrons and gamma rays; a barrel and endcap hadronic calorimeters of total absorption to register the energy of all the hadron particles. The coil is inserted into a 10,000 ton flux-return steel yoke that consists of five three-layered barrel wheels around the coil and several endcap disks on both ends of the coil. The drift tube chambers [4] are installed between the layers of the barrel wheels and serve for measuring the momenta of muons escaping the barrel calorimeters. The muon trajectories are

 doi:10.20944/preprints202410.2201.v1

bent with the steel blocks of the barrel layers magnetized with the solenoid returned magnetic flux. This bending allows the muon momentum measurements with drift tube chambers, and the knowledge of the magnetic flux density distribution in steel blocks of the yoke is a key to the measurement precision. In a similar manner the cathode strip chambers [5] located between the magnetized endcap disks measure the muon momenta in the forward region.

The magnetic flux density inside the solenoid coil has been measured with a special field-mapping machine [6] to a relative precision of 7×10^{-4}. Inside the coil the magnetic flux density is monitored by six nuclear magnetic resonance probes with an averaged precision of $(5.2 \pm 1.3) \times 10^{-5}$ T [7]. In the air gaps between the yoke barrel wheels and on the endcap disks' surfaces, the magnetic flux density is monitored with the three-dimensional (3D) B-sensors (Hall probes) with an averaged precision of $(3.5 \pm 0.5) \times 10^{-5}$ T [7]. The magnetic flux in steel blocks of the magnet flux-return yoke has been calculated by a CMS magnet 3D model [8] based on the program TOSCA (TwO SCAlar potential method) [9], developed in 1979 [10] at the Rutherford Appleton Laboratory. This model reproduces the magnetic flux density distribution measured with the field-mapping machine inside the CMS coil to within 0.1% [11]. The CMS magnetic field map [12] prepared with this model inside a cylinder of 9 m radius has a quasi-rotational symmetry.

To verify the magnetic flux distribution calculated in the yoke steel blocks, direct measurements of the magnetic flux density in the selected regions of the yoke have been performed during the CMS magnet test in 2006 [13] when four fast discharges of the CMS coil (190 s time constant) from the currents of 12.5, 15, 17.55, and 19.14 kA have been triggered manually to test the magnet protection system. These discharges were used to induce voltages with amplitudes of 0.5–4.5 V in 22 flux loops wound around 12 yoke blocks in special grooves, 30 mm wide and 12–13 mm deep. The loops have 7–10 turns of 45 wire flat ribbon cable and the cross-sections of areas enclosed by the flux loops vary from 0.3 to 1.59 m^2 on 10 blocks of the yoke barrel wheels and from 0.5 to 1.12 m^2 on 2 blocks of the yoke endcap disks [14]. An integration technique [15] was developed to reconstruct the average initial magnetic flux density in the cross-sections of these selected steel blocks at full magnet excitation.

At that time, no fast discharge of the CMS magnet from its operational current of 18.164 kA, which corresponds to a central magnetic flux density of 3.81 T, have been performed. To measure the magnetic flux density in the steel blocks of the flux-return yoke at this operational current, seven standard linear discharges of the CMS magnet with a current rate as low as 1–1.5 A/s were performed later [7, 16]. To provide these measurements, the voltages induced in the flux loops (with amplitudes of 20–250 mV) were measured with six 16-bit data acquisition (DAQ) modules and integrated offline over time [7].

In 2022 these modules have been replaced with new 16-bit DAQ system based on the Siemens S7-1500 programmable logic controller (PLC) drives [17]. The new readout boxes had connected each other by the Ethernet cables through the CMS cable chains that allowed to open and close the magnet yoke without disconnection of the DAQ system parts. New organization of the readout scheme has allowed to register two occasionally occurred fast discharges of the CMS coil: one from the operational current of 18.164 kA, and another one from the current of 15.221 kA after the standard discharge of the magnet from the operational current to this value. Both these fast discharges in combination with the fast discharge from 9.5 kA registered in 2017 [16] are used in this study to single out the contribution of the eddy currents into the induced voltages registered in the fast discharges of 2006 and to improve the accuracy of these flux loop measurements.

The article is organized as follows: Section 2 describes the apparatus used for the flux loop measurements and the procedure of the eddy current contribution estimations; Section 3 contains results of the flux loop measurements in the fast discharges of the CMS coil; Section 4 presents a discussion of the obtained results and, finally, conclusions are drawn in Section 5.

Preprints.org (www.preprints.org) | NOT PEER-REVIEWED | Posted: 28 October 2024 doi:10.20944/preprints202410.2201.v1

2. Materials and Methods

2.1. Description of the Flux Loop Measuring System

In Figure 1 an area of the flux loop location in the CMS magnet yoke is shown [7]. The magnetic flux density distribution in this area is described with a color scale from zero to 4 T with a unit of 0.5 T. The positions of the flux loop cross-sections are indicated by the black lines across the magnetized steel blocks. Sixteen flux loops located on ten barrel yoke steel blocks in the 30° azimuthal sector at 270° measure the negative values of the axial magnetic flux density B_z that is orthogonal to the flux loop cross-sections. Six flux loops installed on the 18° azimuthal sector of the endcap disks at 270° measure the positive values of the vertical magnetic flux density B_y that is also orthogonal to the flux loop cross-sections. The Y- and Z-positions of the 3D B-sensors used to monitor the magnetic flux density in the air gaps between the steel blocks are indicated in Figure 1 by small black squares.

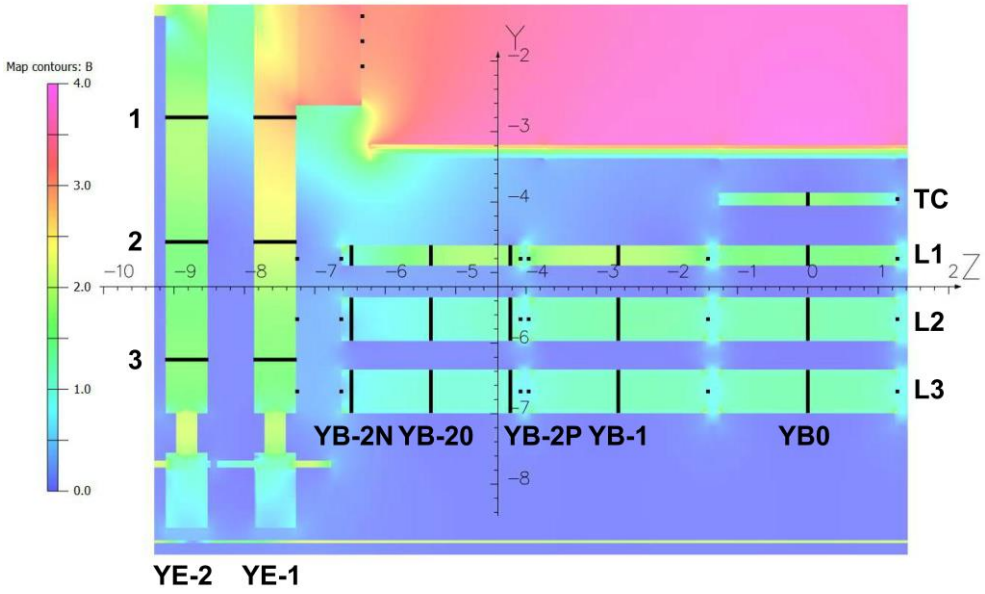

Figure 1. Distribution of the magnetic flux density B in Tesla in the vertical YZ-plane of the flux loop location area [7]. Sixteen flux loops are installed in the 30° azimuthal sector at 270° of the CMS magnet barrel flux-return yoke on four layers (TC, L1, L2, L3) of the central barrel wheel YB0, and on three layers (L1, L2, L3) of the barrel wheels YB−1 and YB−2 at negative Z-coordinates shown in meters on the Z-axis. Six flux loops are wound at the distances 1, 2, 3 along the 18° azimuthal sector at 270° of the CMS endcap thick disks. The black lines indicate the Y- or Z-positions of the loop cross-sections. The small black squares indicate the projections to the YZ-plane of the 3D B-sensor locations installed on the surfaces of the yoke steel blocks.

The coordinate axes shown in Figure 1 represent the CMS coordinate system where the origin of the CMS reference frame is located in the center of the superconducting solenoid coil, the X axis lies in the LHC plane and is directed to the center of the LHC machine, the Y axis is directed upward and is perpendicular to the LHC plane, and the Z axis makes up the right triplet with the X and Y axes and is directed along the vector of magnetic flux density created on the axis of the superconducting coil. The direction of the axial magnetic flux density inside (red area in Figure 1) and outside (blue area in Figure 1) the coil is opposite.

To measure the magnetic flux density induces in steel blocks with the coil returned magnetic flux, the variation of the magnetic flux though the flux loop cross-sections is needed. This variation creates the analog voltage in the wires of each flux loop, and the shape of this voltage $v(t)$ on time t can be described by equation as follows:

$$v(t) = \frac{d\Phi}{dt} = A \cdot N \cdot \frac{dB_i}{dI} \cdot \frac{dI}{dt}. \quad (1)$$

 doi:10.20944/preprints202410.2201.v1

Here Φ is a magnetic flux through the flux loop cross-section, A is an area encircled by the flux loop, N is the number of turns in the flux loop, B_i is either axial B_z or vertical B_y, magnetic flux density component and I is a current in the solenoid winding. To obtain the magnetic flux in the beginning of the variation, the voltage $v(t)$ should be integrated over time of the variation [15]. Dividing the magnetic flux by the flux loop area A and the number of the loop turns N gives the initial magnetic flux density B_i.

To induce the voltages in the flux loops, either a standard magnet ramp downs [16] or the magnet fast discharges [13] from the operating currents could be used. The present analysis is based on seven fast discharges shown in Figure 2 and performed from the magnet currents of 9.5, 12.5, 15, 15.221, 17.55, 18.164, and 19.14 kA. These currents create in the CMS superconducting coil the initial central magnetic flux density B_0 of 2.02, 2.64, 3.16, 3.20, 3.68, 3.81, and 4.01 T, accordingly.

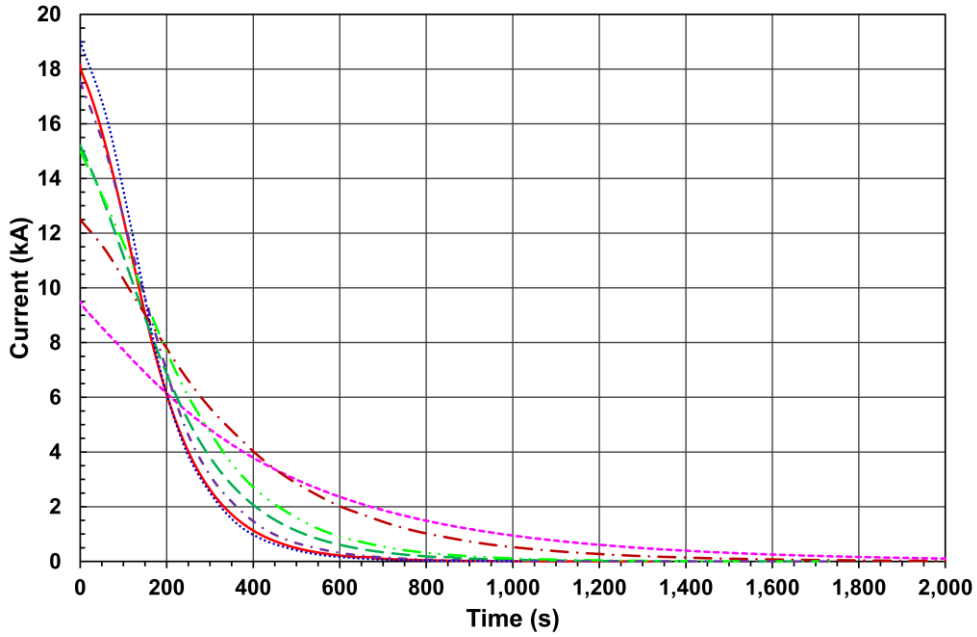

Figure 2. Fast discharges occurred from the CMS magnet currents of 9.5 (magenta short dashes), 12.5 (brown dash-dots), 15 (light green dash-double dots), 15.221 (dark green dashes), 17.55 (violet short dash-dots), 18.164 (red smooth line), and 19.14 (blue dots) kA. These currents create in the CMS superconducting coil the initial central magnetic flux density B_0 of 2.02, 2.64, 3.16, 3.20, 3.68, 3.81, and 4.01 T, accordingly.

The voltages induced in the flux loops have been registered with three different DAQ systems. The first one [14] was used to register the flux loop voltages in the fast discharges performed in 2006 [13] from the CMS magnet currents of 12.5, 15, 17.55, and 19.14 kA. This system included seven USB-based DAQ modules USB-1208LS of Measurement Computing [18] with four differential 12-bit analog inputs each. The USB-1208LS DAQ modules were attached by the USB cables to two network-enabled AnywhereUSB®/5 hubs [19] connected to the personal computer through 3Com® OfficeConnect® Dual Speed Switch 5 [20] sitting on local Ethernet network cable of 90 m. A precision of the signal amplitude measurements with the 12-bit modules was 2.44 mV.

In 2013/2014 this DAQ system has been upgraded by replacing the 12-bit modules with new 16-bit USB-1608G modules from the same manufacturer. This replacement has allowed the signal amplitude measurements with a precision of 0.15 mV [16]. The new 16-bit signal readout gives a resolution of 0.75% at a typical amplitude of 20 mV. The local Ethernet network cable of 90 m has been replaced by the shielded optical fibre cable of 100 m supplied with two Magnum CS14H-12VDC Convertor Switches on both ends. This modification has allowed to perform the flux loops measurements during the CMS magnet standard ramp downs with the current discharge speed as low as 1–1.5 A/s at acceptable accuracy [16,21]. With this system the flux loop voltages induced during the CMS magnet fast discharge from the current of 9.5 kA have been recorded in 2017 [7,16].

 doi:10.20944/preprints202410.2201.v1

The present DAQ scheme developed in 2022 and used to register the flux loop voltages during the CMS magnet fast discharges from the currents of 15.221 and 18.164 kA is displayed in Figure 3.

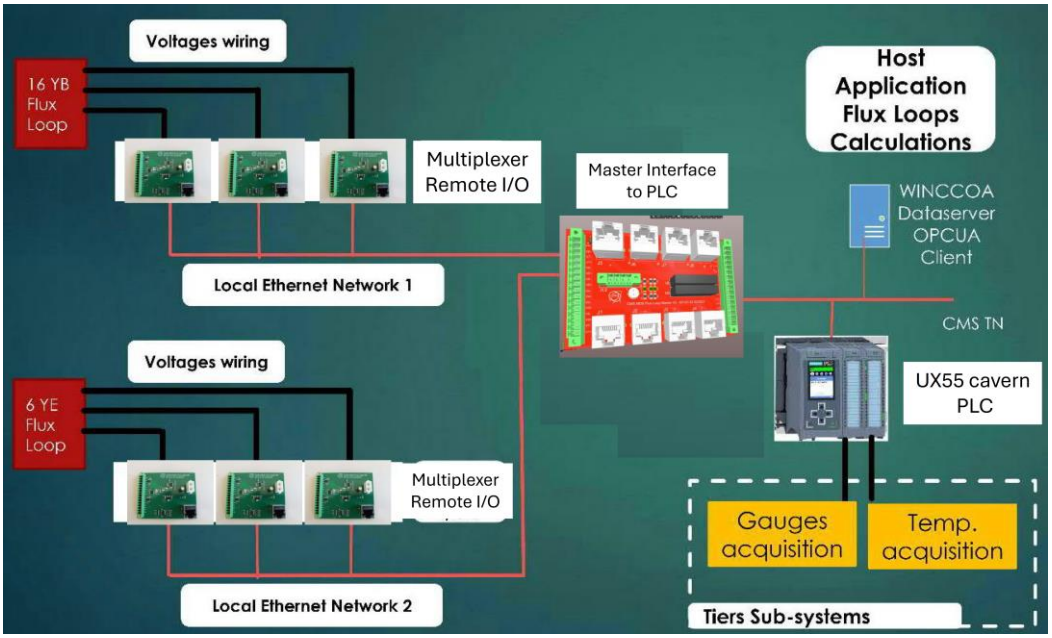

Figure 3. DAQ scheme of the flux loop signals measuring system. The system contains six custom multiplexers assembled in the patch boxes to readout the flux loop induced voltages. Through the custom master PLC interface circuit, the multiplexers relate to Siemens S7-1500 PLC drives to propagate the signals to the WinCC OA software that stores the voltage values in the database.

This DAQ design includes radiation-hard multiplexers assembled with 24 V DC power supplies and Burndy connectors in the custom patch boxes as shown in Figure 4.

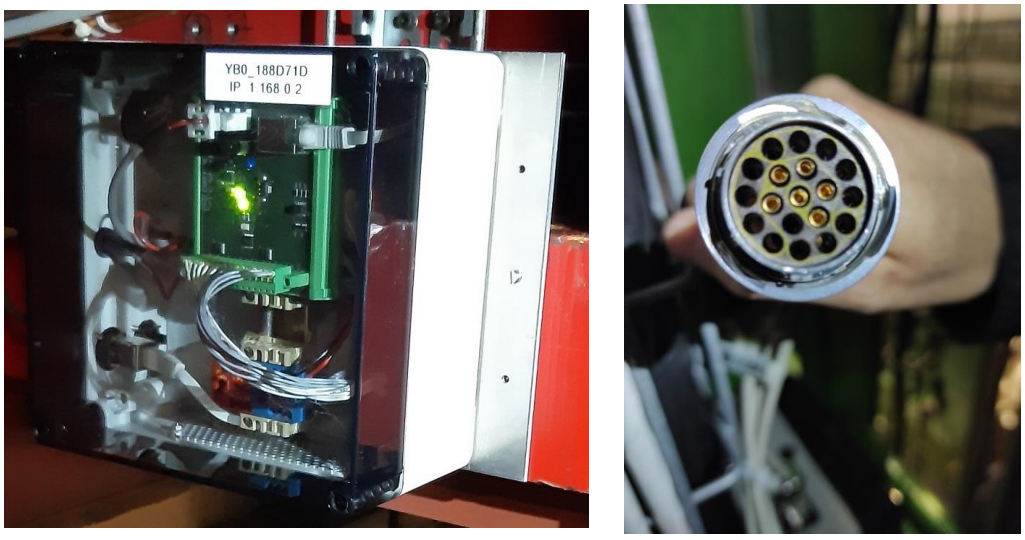

(**a**) (**b**)

Figure 4. Custom multiplexer assembled in the patch box (**a**) with a 24 V DC power supply and the 19-pins Burndy connector (**b**) wiring the flux loops to the multiplexer.

Three, four or six flux loops are wired to each multiplexer through the 19-pins Burndy connector shown in Figure 4b. The multiplexer interface circuit allows to read up to eight channels through the Ethernet cable. All the Ethernet cables from the multiplexers are connected to a main circuit interface, which dispatches the analog signals to the PLC modules and the control bits of the multiplexers to a digital output module. The PLC modules are connected to the Siemens S7-1500 CPU [17] that contains

 doi:10.20944/preprints202410.2201.v1

the readout software and is located outside of the experimental cavern. The information is sending by the PLC through the WinCC OA software and OPC UA driver to the database to be archived.

The fast discharges induce in the flux loops the voltages with rather complicated shapes. The examples of these shapes in the flux loops YB−2P/L2 and YE−2/2 during different fast discharges are shown in Figure 5.

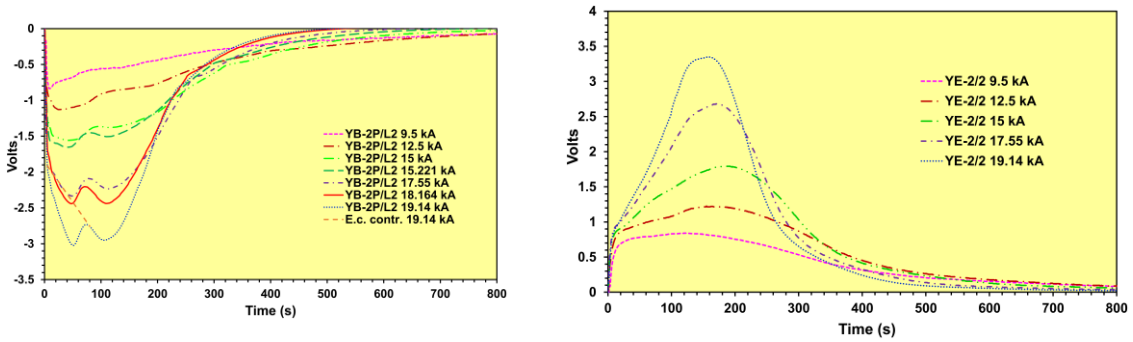

(**a**) (**b**)

Figure 5. (**a**) Voltages measured in the first flux loop P on the L2 layer of the external barrel wheel YB−2 during all seven fast discharges performed from different magnet currents. Orange short-dashed line cuts the contribution of the eddy currents to the signal in the beginning of the magnet fast discharge performed from the current of 19.14 kA. This contribution has been estimated [7] at the level of 4.6% as into the integrated magnetic flux, as into the integrated magnetic flux density; (**b**) Voltages measured in the middle flux loop 2 of the endcap disk YE−2 during five fast discharges performed from different magnet currents.

The voltage shape of each curve shown in Figure 5a have two minima and one extremum between them. The second minima, occurred at 116–185 s from the beginning of the fast discharges, correspond to the inflection points of the curves of the current dependencies on time shown in Figure 2. The first minima, occurred at 9.25–51 s from the beginning of the fast discharges, correspond to the maxima of the eddy currents induced in the steel cross-section of the flux loop YB−2P/L2 by changing the current rate. The eddy currents are damped due to the resistivity of steel near the extrema, occurred at 71–122 s. The area of the signal from the first minimum to extremum describe the eddy current contribution to the induced voltage and is decreasing with increasing the initial currents of the fast discharges. The area separated by the orange short-dashed line from the signal at the fast discharge from the current of 19.14 kA corresponds to the contribution of the eddy current into the induced voltage at the level of 4.6% [7].

2.2. Estimation of the Eddy Current Contribution into the Induced Voltages

To estimate the eddy current contribution more precisely, three fast discharges occurred occasionally during the standard ramp downs of the CMS magnet from the operational current of 18.164 kA are used. These three fast discharges are presented in Figure 6 and have been generated from the currents of 9.5, 15.221, and 18.164 kA. In these measurements the voltages induced in each flux loop according to Eq. (1) are integrated over the entire time of the magnet ramp downs, i. e. during 17,000 (9.5 kA), 4460 (15.221 kA), and 1363 (18.164 kA) s. All these integrations give the initial magnetic fluxes Φ_{FD} in each flux loop cross-section those are compared with the reference magnetic fluxes Φ_{SRD} averaged in each flux loop over the seven measurements performed with the standard magnet ramp downs [7] from the current of 18.164 kA.

Preprints.org (www.preprints.org) | NOT PEER-REVIEWED | Posted: 28 October 2024 doi:10.20944/preprints202410.2201.v1

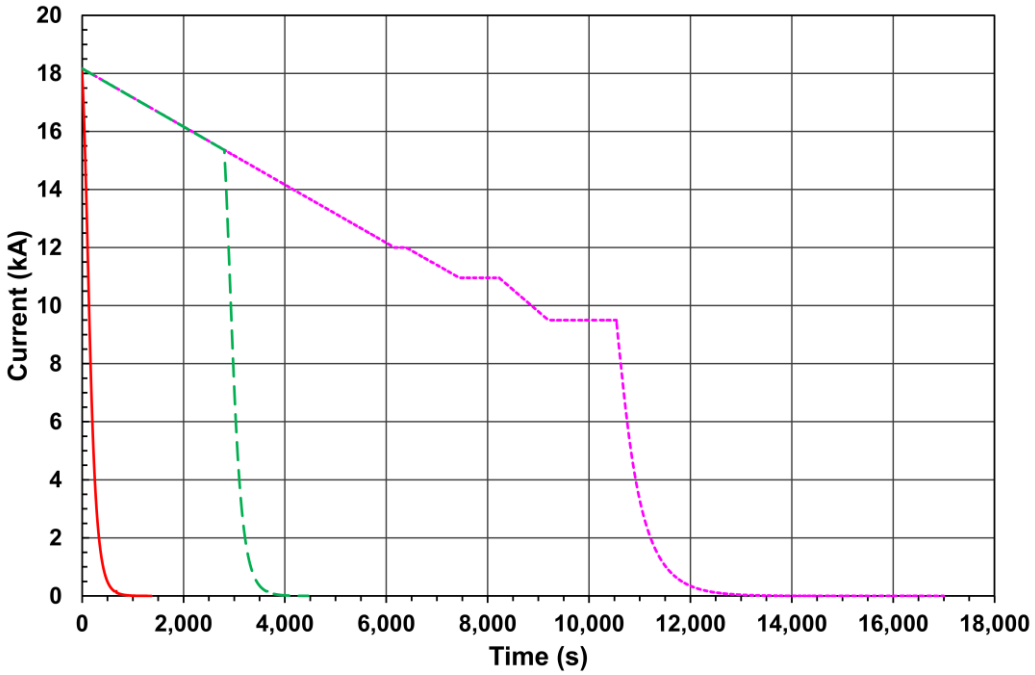

Figure 6. Three fast discharges occasionally occurred from the currents of 9.5 (magenta short-dashes), 15.221 (dark green dashes), and 18.164 (smooth red line) kA during the standard CMS magnet ramp downs with a rate of 1–1.5 A/s.

The results of comparisons for 20 flux loops and for all the seven fast discharges from the currents of 9.5, 12.5, 15, 15.221, 17.55, 18.164, and 19.14 kA are presented in Figure 7.

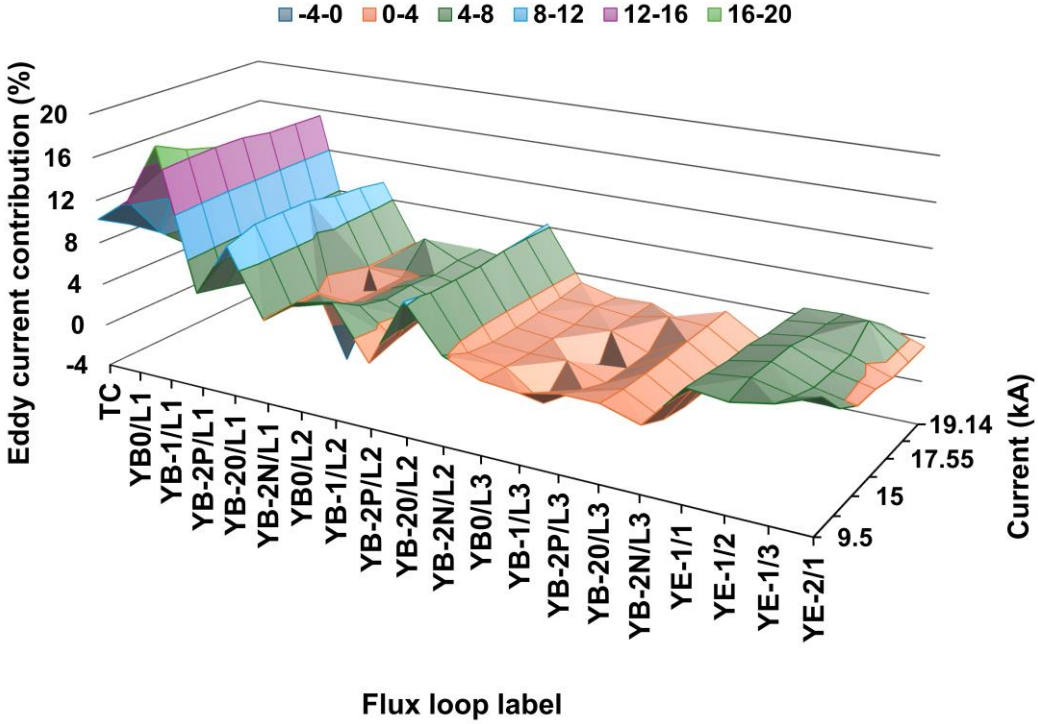

Figure 7. The eddy current contributions to 20 flux loops vs. initial currents of the fast discharges.

The flux loops YE−2/2 and YE−2/3 were disconnected when the fast discharges from the currents of 15.221 and 18.164 occurred. In the further study the contributions of the eddy currents into these flux loop signals are taken from the estimations made for the fast discharge from the current of 9.5 kA.

 doi:10.20944/preprints202410.2201.v1

The estimated contributions of the eddy current, *E.c. contr*, in each flux loop are obtained from a ratio

$$E.c.\ contr = \frac{(\Phi_{FD} - \Phi_{SRD})}{\Phi_{SRD}} \cdot 100\%. \quad (2)$$

Here Φ_{FD} is the magnetic flux through the given flux loop measured with the standard ramp down and subsequent fast discharge of the magnet, and Φ_{SRD} is the magnetic flux through the given flux loop averaged over seven measurements performed with the standard magnet ramp downs. The contributions of the eddy currents for other four initial currents of the fast discharges are obtained by the interpolation and extrapolation of thee estimated *E.c. contr* values using the polynomial of the second order.

The obtained contributions in each flux loop decrease with increasing the initial current values and are in the range from −4.12% (in the flux loop YB−2N/L1 at 15.221 kA) to 18.07% (in the flux loop YB−1/L1 at 9.5 kA). Table 1 presents the values of *E.c. contr* averaged over the flux loops in different yoke layers at each value of the initial current of the fast discharges.

Table 1. Eddy current contributions at the magnet steel yoke layers* during the fast discharges.

Current (kA)	L1&TC	L2	L3	EC−1	EC−2/1	Barrel	Endcap	Yoke
9.5	9.96 ± 5.17	5.53 ± 2.43	2.67 ± 0.47	5.88 ± 0.33	7.50	6.30 ± 4.53	6.28 ± 0.85	6.29 ± 4.04
12.5	8.85 ± 4.73	4.74 ± 2.02	1.66 ± 1.16	5.68 ± 0.40	5.05	5.32 ± 4.29	5.52 ± 0.45	5.36 ± 3.82
15	8.07 ± 4.74	4.37 ± 2.00	1.83 ± 0.94	5.30 ± 0.73	3.77	4.97 ± 4.01	4.92 ± 0.97	4.96 ± 3.58
15.221	6.68 ± 6.81	4.38 ± 2.02	1.81 ± 0.96	5.25 ± 0.75	3.70	4.44 ± 4.60	4.86 ± 0.99	4.53 ± 4.11
17.55	7.43 ± 4.83	4.48 ± 2.04	1.84 ± 0.96	4.94 ± 0.46	3.19	4.76 ± 3.85	4.51 ± 0.95	4.71 ± 3.45
18.164	7.98 ± 5.09	4.86 ± 2.26	1.79 ± 1.56	5.01 ± 0.25	3.16	5.27 ± 4.25	4.39 ± 1.08	5.44 ± 3.80
19.14	7.10 ± 4.89	4.69 ± 2.08	1.93 ± 0.93	4.63 ± 0.15	3.20	4.73 ± 3.77	4.28 ± 0.73	4.64 ± 3.37

* Only 20 flux loops shown in Figure 7 are used.

The effects of decreasing the eddy current contributions from 9.5 to 15 kA of the initial current and a stabilisation of the contributions after 15 kA in each yoke layer are clear visible in Table 1.

3. Results

In Figure 8 the axial B_z (negative) magnetic flux density, or vertical B_y (positive) magnetic flux density components calculated in all the 22 flux loop cross-sections at the CMS coil currents of 9.5, 12.5, 15, 15.221, 17.55, 18.164, and 19.14 kA is displayed. In the barrel layers the minimum absolute B_z value of 0.377 T is reached in the cross-section of the YB−2N/L2 flux loop at the current of 9.5 kA. The maximum absolute value of 2.034 T is achieved in the cross-section of the YB−1/L1 flux loop at the current of 19.14 kA. In the endcap disks the minimum value of 0.947 T is reached in the cross-section of the YE−2/2 flux loop at the current of 9.5 kA. The maximum value of 2.550 T is achieved in the cross-section of the YE−1/1 flux loop at the current of 19.14 kA. The corresponded values measured at the same currents are 0.314 and 2.074 T, and 0.926 and 2.538 T, accordingly.

The axial B_z (negative) magnetic flux density, or vertical B_y (positive) magnetic flux density components measured in all the 22 flux loop cross-sections at the CMS coil currents of 9.5, 12.5, 15, 15.221, 17.55, 18.164, and 19.14 kA is presented in Figure 9.

In Figure 10 the comparisons of measured (*Meas*) and calculated (*Calc*) axial magnetic flux density, or vertical magnetic flux density components in all the 22 flux loop cross-sections at the CMS coil currents of 9.5, 12.5, 15, 15.221, 17.55, 18.164, and 19.14 kA are shown as a ratio *(Meas−Calc)/Calc* (%). The values of this ratio averaged over the flux loops in different yoke layers at each value of the initial current of the fast discharge are presented in Table 2.

 doi:10.20944/preprints202410.2201.v1

Table 2. The ratio *(Meas−Calc)/Calc* (%) at the magnet yoke layers* for the different initial currents.

Current (kA)	L1&TC	L2	L3	EC−1	EC−2	Barrel	Endcap	Yoke
9.5 (new)	**−3.60 ± 4.91**	**−4.71 ± 7.74**	**−7.39 ± 10.45**	**2.77 ± 3.38**	**4.98 ± 6.87**	**−5.13 ± 7.47**	**3.88 ± 4.99**	**−2.67 ± 7.92**
12.5 (old)	−0.76 ± 10.15	7.65 ± 8.51	−2.85 ± 10.79	0.69 ± 5.51	3.24 ± 2.22	1.22 ± 10.27	1.97 ± 4.01	1.42 ± 8.91
15 (old)	2.30 ± 2.77	5.39 ± 7.27	−2.44 ± 9.45	1.59 ± 2.37	2.29 ± 3.97	1.78 ± 7.13	1.94 ± 2.95	1.82 ± 6.20
15.221 (new)	**0.22 ± 1.30**	**−2.61 ± 6.81**	**−5.73 ± 8.44**	**1.09 ± 1.08**	**1.61 ± 7.57**	**−2.52 ± 6.19**	**1.35 ± 4.84**	**−1.46 ± 6.01**
17.55 (old)	3.16 ± 2.37	3.48 ± 5.53	−2.47 ± 8.58	1.03 ± 1.06	1.14 ± 4.15	1.50 ± 6.11	1.08 ± 2.71	1.39 ± 5.33
18.164 (new)	***−0.39 ± 0.84***	***−4.58 ± 6.01***	***−6.48 ± 8.17***	***0.09 ± 0.23***	***2.62 ± 3.29***	***−3.60 ± 5.91***	***1.36 ± 2.50***	***−2.25 ± 5.62***
19.14 (old)	1.66 ± 1.99	0.78 ± 5.07	−3.66 ± 8.21	0.14 ± 0.67	−0.13 ± 4.37	−0.27 ± 5.64	0.005 ± 2.80	−0.20 ± 4.96

* All the 22 flux loops shown in Figure 10 are used. The eddy current contributions into the YE−2/2 and YE−2/3 flux loop measurements are taken from the estimations done at the current of 9.5 kA.

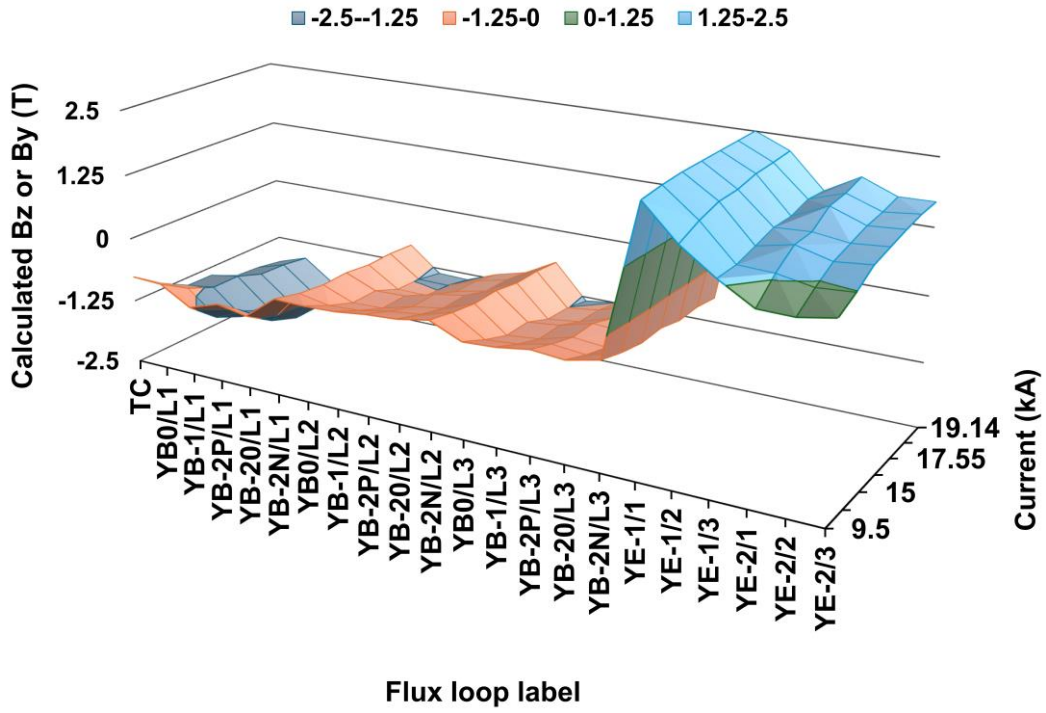

Figure 8. Initial axial B_z (negative) magnetic flux density, or vertical B_y (positive) magnetic flux density components calculated in all the 22 flux loop cross-sections at the CMS coil currents of 9.5, 12.5, 15, 15.221, 17.55, 18.164, and 19.14 kA.

Preprints.org (www.preprints.org) | NOT PEER-REVIEWED | Posted: 28 October 2024 doi:10.20944/preprints202410.2201.v1

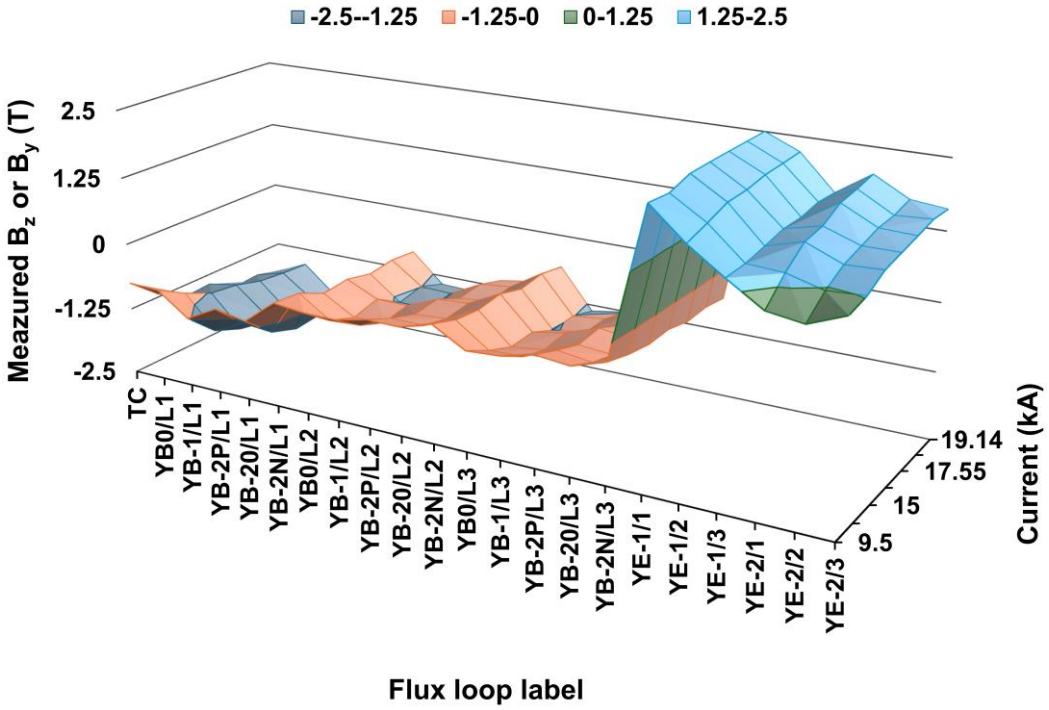

Figure 9. Initial axial B_z (negative) magnetic flux density, or vertical B_y (positive) magnetic flux density components measured in all the 22 flux loop cross-sections at the CMS coil currents of 9.5, 12.5, 15, 15.221, 17.55, 18.164, and 19.14 kA. The eddy current contributions are subtracted from the integrated flux loop induced voltages.

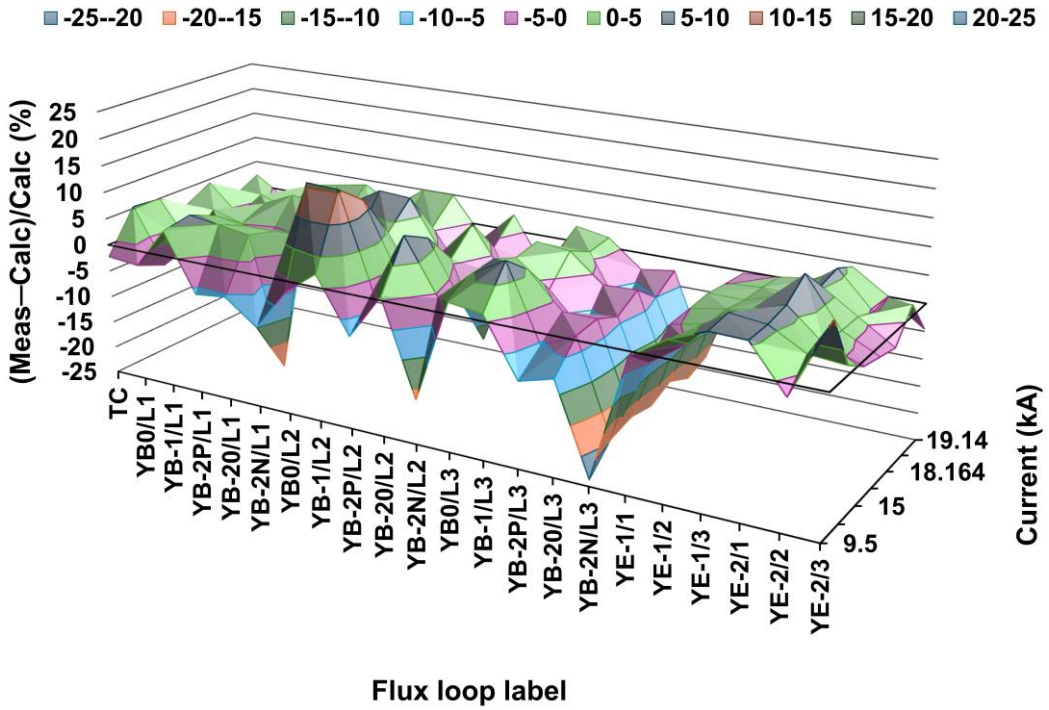

Figure 10. Comparison of measured and calculated axial B_z magnetic flux density, or vertical B_y magnetic flux density components in all the 22 flux loop cross-sections at the CMS coil currents of 9.5, 12.5, 15, 15.221, 17.55, 18.164, and 19.14 kA.

Table 2 contains two sets of comparisons for the new (for the initial currents of 9.5, 15.221, and 18.164 kA) and old (for the initial currents of 12.5, 15, 17.55, and 19.14 kA) flux loop measurements.

 doi:10.20944/preprints202410.2201.v1

Comparisons for the new measurements are highlighted in bold as the reference measurements for the eddy current contribution estimations. The line at the current of 18.164 kA, highlighted in italics, exactly corresponds to the comparisons of the measured and calculated magnetic flux density values obtained with averaging the seven sets of measurements performed with the standard CMS magnet ramp downs [7]. Comparisons for the four old measurements presented in Table 2 are obtained from the set of the fast discharges made in 2006 considering the present eddy current contribution estimations.

From this Table one can observe a systematic difference between the new and old sets of measurements that reflects a different precision of the apparatus used to readout the voltages in 2006 (12-bit DAQ modules) and from 2015 (16-bit DAQ modules). The values of the (*Meas*−*Calc*)/*Calc* ratio with the error bars presented in the last three columns of Table 2 are displayed in Figure 11 that illustrates the systematic difference between two sets of the flux loop measurements. In general, the difference between the measured and calculated values of the magnetic flux density in the CMS yoke steel blocks makes up several percent.

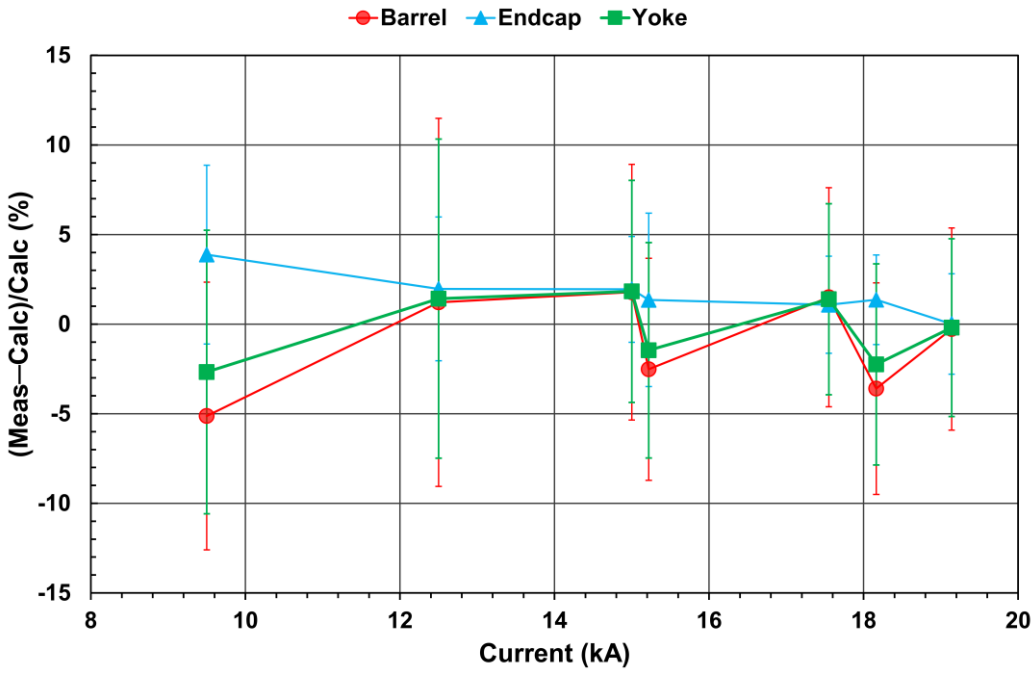

Figure 11. Averaged comparison of measured and calculated axial magnetic flux density, B_z (in the 16 barrel flux loops), or vertical magnetic flux density, B_y (in the 6 endcap flux loops), as well as of both components in all the 22 flux loop cross-sections (yoke) versus the CMS coil currents of 9.5, 12.5, 15, 15.221, 17.55, 18.164, and 19.14 kA. The currents of 9.5, 15.221, and 18.164 kA are the reference currents where the eddy currents contributions are obtained directly from the data.

In 2018 the flux loops measurements made in 2006 with the fast discharges from the currents of 17.55 and 19.14 kA have been revised using the eddy current contribution estimations obtained with the fast discharge from the current of 9.5 kA occurred in 2017 [16] in the end of the CMS magnet standard ramp down from the operational current of 18.164 kA. That time the following values of the (*Meas*−*Calc*)/*Calc* ratio have been obtained: 0.55 ± 5.98 % in the barrel layers and −0.07 ± 1.56 % in the endcap disks at the current of 17.55 kA; −1.08 ± 5.52 % in the barrel layers and 1.28 ± 1.71 in the endcap disks at the current of 19.14 kA. These values are compatible with the new corresponded values of 1.50 ± 6.11 % (barrel layers) and 1.08 ± 2.71 % (endcap disks) at 17.55 kA, and −0.27 ± 5.64 % (barrel layers) and 0.005 ± 2.80 % (endcap disks) at 19.14 kA, which confirms the validity of the new procedure used to estimate the contributions of eddy currents.

 doi:10.20944/preprints202410.2201.v1

4. Discussion

To explain the obtained differences between the measured and calculated values of the magnetic flux density in the CMS yoke steel blocks and to find a reason for that, consider the (*Meas−Calc*)/*Calc* ratio in each flux loop cross-section. Figure 12 shows the comparison of measured and calculated axial magnetic flux density, B_z, or vertical magnetic flux density, B_y, in each of the 22 flux loop cross-sections performed in two sets of measurements: new measurements with the fast discharges from 9.5, 15.221, and 18.164 kA and old measurements with the fast discharges from 12.5, 15, 17.55, and 19.14 kA. In this Figure both sets are combined as well, and the independent measurements performed in the air gaps between the barrel wheels with the 3D B-sensors [7] are added. The curves in Figure 12 show clearly large discrepancies between the measured and calculated values in the cross-sections of the flux loops near the "negative" (N) edge of the barrel wheel YB−2 in all three layers. This edge is looking inside the large gap between the barrel wheel YB−2 and the endcap disk YE−1 as is shown in Figure 1.

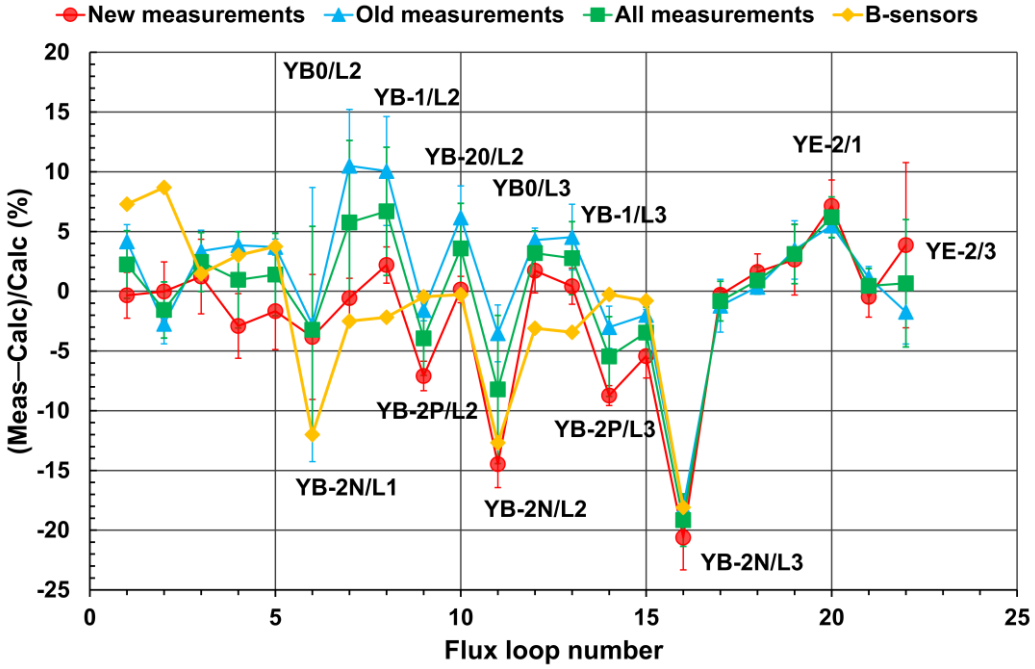

Figure 12. Comparison of measured and calculated axial magnetic flux density, B_z, or vertical magnetic flux density, B_y, in each of the 22 flux loop cross-sections performed in different sets of measurements: new measurements at 9.5, 15.221, and 18.164 kA; old measurements at 12.5, 15, 17.55, and 19.14 kA, and both new and old (all) measurements. The comparisons of the axial magnetic flux density measured with 3D B-sensors [7] and calculated with the CMS magnet model [8] are also displayed.

The 3D B-sensors located at the edges of each layer of the YB−2 wheel also indicate a discrepancy between the calculated and measured axial magnetic flux density. Since the flux loop and B-sensor measurements are independent, the only explanation for these discrepancies is that the CMS magnet model does not describe the magnetic flux well enough in this region. To assess the influence of this effect on the (*Meas−Calc*)/*Calc* ratio, the three flux loops YB−2N/L1, YB−2N/L2, and YB−2N/L3 were excluded from consideration. With this approach the values of the (*Meas−Calc*)/*Calc* ratio became in the barrel wheel layers as 3.03 ± 3.51 % at 17.55 kA, and 1.46 ± 2.89 % at 19.14 kA. This makes the measurements and calculations compatible within 3%. The (*Meas−Calc*)/*Calc* ratio is less than 1.5% in 9.1% (the fast discharge from 12.5 kA) to 68.2% (the fast discharge from 18.164 kA) of the flux loop cross-sections, and between 1.5% and 3% in 4.5% (the fast discharge from 18.164 kA) to 36.4% (the fast discharge from 19.14 kA) of the flux loop cross-sections. In contrast, the magnetic flux density distribution in the CMS tracking volume is perfectly homogeneous [22] and is described with the CMS magnet 3D model [8] to within 0.1% [11].

 doi:10.20944/preprints202410.2201.v1

5. Conclusions

In this study, the verification of the Compact Muon Solenoid (CMS) magnetic field map in the flux-return magnet yoke steel layers is performed using the magnetic flux density measurements in 22 cross-sections of the flux loops mounted on 12 yoke steel blocks. Seven fast discharges generated by the CMS coil currents of 9.5, 12.5, 15, 15.221, 17.55, 18.164, and 19.14 kA made it possible to record the flux loops voltages induced by the rapid magnetic flux decay in the flux loop regions and to reconstruct the initial magnetic flux density in the flux loop cross-sections by the off-line integration of these voltages over time. A new method is applied to estimate the contributions to the induced voltages from the eddy currents generated in steel by the fast discharges. The contribution of eddy currents to the flux loop signals reaches 18.07% and decreases to less than 1% for some flux loops with an increase of the fast discharge initial current. A comparison of the measured and calculated magnetic flux density values in steel shows their compatibility within 3%. In contrast, the magnetic flux density distribution in the CMS tracking volume is described by the three-dimensional model of the CMS magnet with an accuracy of 0.1%.

Author Contributions: Technical coordination, A.G.; conception, V.K.; engineering integration, B.C., A.G., A.K., M.O. and X.P.; flux loop electronics, A.K., M.O. and X.P.; flux loop read-out software, A.K., M.O. and X.P.; flux loop measurements, B.C., A.K., V.K., M.O. and X.P.; data analysis, V.K.; writing—original draft preparation, V.K.; writing—editing, V.K. All authors have read and agreed to the published version of the manuscript.

Funding: This research received no external funding.

Data Availability Statement: No data are available.

Acknowledgments: The authors are extremally grateful to the CMS Technical Coordinators Alain Hervé, Austin Ball, Wolfram Zeuner, and Paola Tropea of CERN for several years of interest to these studies and fruitful discussions.

Conflicts of Interest: The authors declare no conflict of interest.

References

1. CMS Collaboration. The CMS experiment at the CERN LHC. *J. Instrum.* **2008**, *3*, S08004. https://doi.org/10.1088/1748-0221/3/08/S08004.
2. Evans, L.; Bryant, P. LHC Machine. *J. Instrum.* **2008**, *3*, S08001. https://doi.org/10.1088/1748-0221/3/08/s08001.
3. Hervé, A. Constructing a 4-Tesla large thin solenoid at the limit of what can be safely operated. *Mod. Phys. Lett. A* **2010**, *25*, 1647–1666. https://doi.org/10.1142/S0217732310033694.
4. CMS Collaboration. Performance of the CMS drift tube chambers with cosmic rays. *J. Instrum.* **2010**, *5*, T03015, https://doi.org/10.1088/1748-0221/5/03/T03015.
5. CMS Collaboration. Performance of the CMS cathode strip chambers with cosmic rays. *J. Instrum.* **2010**, *5*, T03018, https://doi.org/10.1088/1748-0221/5/03/T03018.
6. Klyukhin, V.; Ball, A.; Bergsma, F.; Campi, D.; Curé, B.; Gaddi, A.; Gerwig, H.; Hervé, A.; Korienek, J.; Linde, F.; et al. Measurement of the CMS Magnetic Field. *IEEE Trans. Appl. Supercond*. **2008**, *18*, 395–398. https://doi.org/10.1109/TASC.2008.921242.
7. Klyukhin, V.; Ball, A.; Bergsma, F.; Boterenbrood, H.; Curé, B.; Dattola, D.; Gaddi, A.; Gerwig, H.; Hervé, A.; Loveless, R.; et al. The CMS Magnetic Field Measuring and Monitoring Systems. *Symmetry* **2022**, *14*, 169. https://doi.org/10.3390/sym14010169.
8. Klyukhin, V. Design and Description of the CMS Magnetic System Model. Symmetry **2021**, *13*, 1052. https://doi.org/10.3390/sym13061052.
9. *TOSCA/OPERA-3d 18R2 Reference Manual*; Cobham CTS Ltd.: Kidlington, UK, 2018; pp. 1–916.
10. Simkin, J.; Trowbridge, C. Three-dimensional nonlinear electromagnetic field computations, using scalar potentials. In *IEE Proceedings B Electric Power Applications;* Institution of Engineering and Technology (IET): London, UK, **1980**; *127*, 368–374. https://doi.org/10.1049/ip-b.1980.0052.
11. Klyukhin, V.I.; Amapane, N.; Andreev, V.; Ball, A.; Curé, B.; Hervé, A.; Gaddi, A.; Gerwig, H.; Karimaki, V.; Loveless, R.; et al. The CMS Magnetic Field Map Performance. *IEEE Trans. Appl. Supercond*. **2010**, *20*, 152–155. https://doi.org/10.1109/TASC.2010.2041200.
12. Amapane, N.; Klyukhin, V. Development of the CMS Magnetic Field Map. *Symmetry* **2023,** *15*, 1030. https://doi.org/10.3390/sym15051030.

13. Campi, D.; Curé, B.; Gaddi, A.; Gerwig, H.; Hervé, A.; Klyukhin, V.; Maire, G.; Perinic, G.; Bredy, P.; Fazilleau, P.; et al. Commissioning of the CMS Magnet. *IEEE Trans. Appl. Supercond*. **2007**, *17*, 1185–1190. https://doi.org/10.1109/TASC.2007.897754.
14. Klyukhin, V.I.; Amapane, N.; Ball, A.; Curé, B.; Gaddi, A.; Gerwig, H.; Mulders, M.; Hervé, A.; Loveless, R. Measuring the Magnetic Flux Density in the CMS Steel Yoke. *J. Supercond. Nov. Magn*. **2012**, *26*, 1307–1311. https://doi.org/10.1007/s10948-012-1967-5.
15. Klyukhin, V.; Campi, D.; Curé, B.; Gaddi, A.; Gerwig, H.; Grillet, J.P.; Hervé, A.; Loveless, R.; Smith, R.P. Developing the Technique of Measurements of Magnetic Field in the CMS Steel Yoke Elements with Flux-loops and Hall Probes. *IEEE Trans. Nucl. Sci*. **2004**, *51*, 2187–2192. https://doi.org/10.1109/TNS.2004.834722.
16. Klyukhin, V., Curé, B., Amapane, N., Ball, A., Gaddi, A., Gerwig, H., Hervé, A., Loveless, R., Mulders, M. Using the Standard Linear Ramps of the CMS Superconducting Magnet for Measuring the Magnetic Flux Density in the Steel Flux-Return Yoke. *IEEE Trans. Magn*. **2019**, *55*, 8300504. https://doi.org/10.1109/TMAG.2018.2868798.
17. Siemens AG Digital Industries. Functional manual SIMATIC S7-1500; A5E03735815-AL; SIEMENS: Nurnberg, Germany, 2023; Available online: https://support.industry.siemens.com/cs/attachments/59192925/s71500_communication_function_manual_en-US_en-US.pdf (accessed on 25 July 2024).
18. *Measurement Computing Corporation*, Norton, MA, USA.
19. *Digi International Inc.*, Minnetonka, MN, USA.
20. *3Com Corporation*, Marlborough, MA, USA.
21. Klyukhin, V.I., Amapane, N., Ball, A., Curé, B., Gaddi, A., Gerwig, H., Mulders, M., Hervé, A., Loveless, R. Flux Loop Measurements of the Magnetic Flux Density in the CMS Magnet Yoke. *J. Supercond. Nov. Magn.* **2017**, *30*, 2977–2980. https://doi.org/10.1007/s10948-016-3634-8.
22. Klyukhin, V.; on behalf of the CMS Collaboration. Influence of the high granularity calorimeter stainless steel absorbers onto the Compact Muon Solenoid inner magnetic field. *SN Appl. Sci*. **2022**, *4*, 235. https://doi.org/10.1007/s42452-022-05122-9.